Marine Pollution Bulletin 227 (2026) 119505

Contents lists available at ScienceDirect

Marine Pollution Bulletin

journal homepage: www.elsevier.com/locate/marpolbul

Tracking the photooxidation products of primary plastic pellets (nurdles) in seawater

Xiangtao Jiang [a], Kaijun Lu [a,b], Zhanfei Liu [a,*]

[a] University of Texas Marine Science Institute, 750 Channel View Drive, Port Aransas, TX, 78373, United States of America
[b] Coastal Carolina University, 100 Chanticleer Dr E, Conway, SC, 29528, United States of America

ARTICLE INFO

Keywords:
Nurdle
Microplastic
Nanoplastic
Photodegradation
LC/MS
Dissolved organic matter

ABSTRACT

Marine plastic debris often undergoes photooxidation through sunlight exposure, potentially releasing photo-oxidized products to the surrounding seawater that may impact ecosystem health and carbon cycling. However, the molecular size and composition of leached products as dissolved organic carbon (DOC) remain poorly understood. In this study, we investigated photooxidation dynamics of two common plastic types — polyethylene (PE) and polycarbonate (PC) pellets, or nurdles, in seawater through 8-week laboratory simulations, representing 3 years of natural sunlight exposure along the Texas coast. This exposure facilitated the leaching of photo-oxidized products as DOC to seawater, with PE nurdles releasing more DOC than PC nurdles by an 18-fold difference due to the difference in their molecular structure, which introduced further differences in their light and oxygen exposure during the incubation. No nano-sized plastic particles (1 nm-0.75 μm) were detected based on the analyses using ultrafiltration (3 k Da cut-off). High-resolution mass spectrometry analysis further revealed that sunlight exposure increased the number of molecular formulas in the plastic-derived DOC, with their stoichiometry reflecting the polymers' chemical compositions. The oxygen-to-carbon ratio in PE-derived DOC increased over time, while the hydrogen-to-carbon ratio in PC-derived DOC decreased, indicating an enrichment of oxygenated compounds, likely due to an increase in carboxyl groups on nurdle surface during the later stages of photooxidation. Collectively, these findings highlight the role of photooxidation in driving the release of small soluble organic molecules, not nano-sized particles from plastics, providing new insights into the photooxidation products and their impacts on marine ecosystems.

Synopsis: We systematically investigated the production and composition of dissolved organic carbon in seawater from polyethylene and polycarbonate nurdles by photooxidation. All the dissolved organic molecules produced were truly dissolved, and they became more oxygenated as photooxidation proceeded.

1. Introduction

The widespread presence of microplastics (< 5 mm) in the environment is a growing concern to the health of ecosystems and public. Microplastics in the environment are contributed by complex and diverse sources, including both primary and secondary. In addition, microplastics are made from a large variety of polymers and contain many different types of additives. These factors make it challenging to study environmental behaviors of microplastics, but plastic pellets, also known as nurdles (1–5 mm diameter), is a good model plastic because they contain little or no additive which makes data interpretation easy, and they are environmentally relevant. As pre-production building blocks, nurdles are manufactured to facilitate the transportation and molding for final plastic products (Hammer et al., 2012), and frequent spilled to the environment due to lack of regulation (de Vos et al., 2021; Sewwandi et al., 2023; Tunnell et al., 2020). Reports of nurdle pollution dated back to as early as 1970s (Carpenter and Smith, 1972). Once spilled, nurdles are readily transported by various environmental forces, such as wind and ocean currents, and accumulate in marine environments due to their resistance to weathering (Acampora et al., 2017; Jiang et al., 2022). It is estimated that over 230,000 tons of nurdles enter the marine environment annually (de Vos et al., 2021).

Like any other microplastics, nurdles in the water not only present physical threat but also chemical hazard to marine life, with documented ingestion by marine fish, birds, and turtles (Clukey et al., 2017; Gregory, 2009; Ryan, 1988). Moreover, analyses of nurdles collected

* Corresponding author.
E-mail address: zhanfei.liu@utexas.edu (Z. Liu).

https://doi.org/10.1016/j.marpolbul.2026.119505
Received 17 June 2025; Received in revised form 26 February 2026; Accepted 27 February 2026
Available online 11 March 2026

from the environment have revealed the presence of harmful contaminants, including Polycyclic Aromatic Hydrocarbons (PAHs), Polychlorinated Biphenyls (PCBs), and mercury, further underscoring the complex risks they pose to marine ecosystems (Antunes et al., 2013; Endo et al., 2005; Jiang et al., 2022; Zhang et al., 2015).

Nurdles in marine environments are made of a variety of polymer types, with polyethylene (PE) and polypropylene (PP) as the most commonly reported (Jiang et al., 2021; Zhang et al., 2015). These pellets undergo weathering from different environmental stressors, such as sunlight, wave action, biofouling, and temperature shifts (Fotopoulou and Karapanagioti, 2012; Turner and Holmes, 2011). Environmental oxidation introduces oxygen into the polymer chains, leading to discoloration, fragmentation, and the release of degradation byproducts into the marine environment (Alimi et al., 2021; Andrady, 2022). For example, the photodegradation of disposable polystyrene lids releases numerous nano-sized plastic fragments (Biber et al., 2019; Kuzina and Mikhailov, 2001, 1998, 1993; Lambert and Wagner, 2016; Tang et al., 2022). Moreover, sunlight exposure to various plastics, including PE, PP, and polystyrene (PS), leads to the release of dissolved organic matter (DOM) into the environment (Chen et al., 2019; Egea et al., 2024; Kuman et al., 2024; Lee et al., 2020; Romera-Castillo et al., 2022; Walsh et al., 2021; Ward et al., 2019; Zhu et al., 2020b). Despite these findings, inconsistencies remain regarding the kinetics and fluxes of plastic-derived DOM. Also, prior studies have predominantly focused on quantifying the concentration of DOM produced by small-sized microplastics (1 μm – 5 mm) manufactured through various processes, while overlooked larger-sized plastics (Chen et al., 2019; Ward et al., 2019). In addition, small-sized microplastics are often made by manually grinding and trimming, to ensure size uniformity (Zhu et al., 2020b). This pretreatment, while ensuring size consistency, can cause physical damage to the plastics and expose fresh interiors, thereby complicating direct comparisons across different polymer types. Consequently, there exists a large variability in degradation rates and the fluxes of DOM produced by different polymers. The kinetics and molecular level information of DOM leached from plastics also remain poorly understood.

High resolution mass spectrometry (HRMS) has been used to analyze plastic-derived DOMs. For example, Li et al. (2022). identified hundreds of features from leachates across various plastic polymers using Liquid Chromatography Mass Spectrometer (LC/MS). However, despite these efforts, information regarding nanoplastic constituents within plastic-derived DOMs remains scarce, which may be due to challenges associated with isolating nanoplastics for HRMS analysis, compounded by the inherent poor water solubility of nanoplastic particles. Thus, the characteristics and composition of DOM leached from plastics, spanning from nano to truly dissolved substances, remain largely unexplored. Meanwhile, evidence suggests that plastic-derived DOMs influence microbial activities in the water (Zhu et al., 2020b). Given the increasing prevalence of plastic debris and the critical role of marine DOM in global carbon cycling as a reservoir of potentially bioactive carbon (Hansell and Carlson, 2014), it is of great importance to deepen our understanding of how plastic degradation products affect the marine DOM dynamics.

The goals of this work were to (1) understand the effects of photooxidation on the quantity and composition of leached substances from plastics, and (2) determine whether the leached DOM exists as nano-size particles or truly dissolved compounds. We conducted photooxidation experiments using two types of nurdles as ideal model plastics to work with and commonly encountered in the environment: buoyant PE and non-buoyant polycarbonate (PC) nurdles, under simulated sunlight exposure. We employed Fourier-transform infrared spectroscopy (FTIR) to detect changes in the surface chemistry of the nurdles, focusing on the formation of oxygen-containing functional groups. We also assessed the molecular formula and elemental stoichiometry of plastic-derived DOM through high-resolution LC/MS. Although this work is focused on nurdles, results offer insights into other types of plastics in the environment.

2. Materials and methods

2.1. Polymer materials

High-density polyethylene (HDPE) and polycarbonate (PC) plastic nurdles (~4 mm in diameter) were purchased from a commercial supplier (Polly Plastics), and their composition was confirmed via Fourier transform infrared spectroscopy (FTIR, Shimadzu). HDPE and PC were chosen due to their widespread global production and distinct densities, as HDPE nurdles are buoyant on seawater, while PC nurdles are denser and sink in seawater. Prior to experiments, the nurdles were cleaned in 1% hydrogen peroxide solution followed by ultrasonication for 10 min, after which they were dried in a 60 °C oven for 24 h. Organic additives were not detectable by pyrolysis gas chromatography mass spectrometry (Jiang et al., 2024), which is not unexpected considering that nurdles are virgin plastics.

2.2. Photooxidation experiment

Photooxidation experiments were conducted in a solar simulator (Q-SUN Xe-1) with nurdles immersed in artificial seawater. All exposure experiments were conducted in upright quartz bottles under top-down illumination, but the walls are covered with built-in mirrors, thus the irradiation should be relatively uniform within the chamber. The artificial seawater (salinity: 33 ppt) was prepared by dissolving pre-combusted artificial sea salt (Instant Ocean; 450 °C, 3 h) in pure water, to ensure there is no background DOC (below detection limit, < 30 ppb C) or biological activities in the incubation. Note that the sea salts used contain all the major ions but without nitrate and phosphate. For the light treatment, 1 g of cleaned nurdles (~30 PE or ~ 50 PC) was incubated in 110 mL of artificial seawater within pre-combusted 120 mL quartz bottles, leaving 10 mL of headspace. This recipe was selected to ensure enough DOC produced by photooxidation for later chemical characterization. The solar simulator (Q-SUN Xe-1) provided continuous artificial sunlight at 5000 μmol photons/m^2/s without a light/dark cycle, maintaining a temperature of 33 ± 2 °C by a cooling system in the solar simulator. The total broadband UV (300-400 nm; 1.89 × 10^7 J/m^2/day) dose is about 19 times the daily outdoor total UV dose of Port Aransas, TX (0.9–1.1 × 10^6 J/m^2/day; Wang et al., 2020), i.e., one light-incubation day equated to ~19 days of natural sunlight. The dark treatment followed the same procedure using pre-combusted amber glass bottles stored in a closed box at the same temperature. Triplicate bottles were used for each experiment group. The bottles were manually shaken for 10 s daily and briefly opened (5 s) to balance pressure.

At each sampling point (day 1, weeks 1, 2, 4, 6, and 8), nurdles were recovered by filtration through a pre-combusted 0.7 μm glass fiber filter, rinsed with pure water, and air-dried under a fume hood. Filtrates were divided for analysis, with 20 mL used for bulk DOC measurement via a Shimadzu TOC-V analyzer and the remaining portion stored for further characterization.

The consumption of dissolved oxygen (DO) during the photooxidation was also evaluated in a separate set of experiments but with the same protocol, except that the pre-combusted quartz bottles were filled without headspace to prevent gas exchange. For the dark treatment, the same setup was used, but the quartz bottles were wrapped in aluminum foil to block light. DO was measured in weeks 1 and 2.

2.3. Nurdle characterizations

The weight of nurdles was measured through balance, and the color of nurdles was recorded via a phone camera at each sampling timepoint. FTIR (IRTracer-100, Shimadzu) equipped with an attenuated total reflectance (ATR) accessory was used to assess the photooxidation extent of nurdles. The FTIR spectra were recorded in the range of 4000 to 700 cm^{-1} at a resolution of 8 cm^{-1}, averaging 32 scans. The oxidation degree of a given nurdle was quantified using the FTIR spectrum

according to published methods (Brandon et al., 2016; Jiang et al., 2022). Specifically, oxidation was assessed by quantifying characteristic absorption bands associated with oxygen-containing functional groups, including O—H (hydroxyl), C—O (ether), C═O (carbonyl), and C═C (vinyl). The oxidation index represents the combined contribution of these functional group indices, each calculated by normalizing the maximum absorbance of the corresponding band to a polymer-specific reference peak.

Scanning electron microscopy (SEM, JEOL 6490) was applied to measure the surface morphology of the nurdles. Two nurdles were randomly selected from the samples at each time point and then placed on double-sided carbon tape and coated with 2 nm of carbon powder to enhance conductivity. The SEM was operated at 17 kV under high vacuum, with magnifications ranging from 25× to 300×, recording a detailed examination of the surface appearance with a resolution about 0.5–1 μm. For each individual sample, four images were captured, and the image with the best resolution for each magnification was selected and reported.

2.4. Identification of nanoplastics

To quantify nanoplastics in the solution, 50 mL of the filtrated water sample after photooxidation was ultrafiltered using centrifugal filter (Centricon® Plus, 3 kDa). The cut-off of 3 kDa translates to a globular diameter of about 1–3 nm for an organic molecule (Stolpe et al., 2010). The DOC concentrations of the permeate (< 1 nm) and concentrate (1 nm – 0.75 μm) were measured by a TOC analyzer (Shimadzu TOC-V). The concentration difference between the concentrate and permeate was used to calculate the amount of nanoplastics in the solution. Ultrafiltration was only performed on samples with high DOC concentrations, i.e., PE nurdles of 4, 6, 8 weeks, and PC nurdles of 8 weeks of photooxidation. The detection limit of nanoplastics is constrained by the DOC analyzer, with about 30 μg/L. It should be noted that, in the absence of nanoplastic calibration standards, the ultrafiltration–TOC approach provides a qualitative assessment of nanoplastic presence rather than an absolute quantification.

2.5. DOC extraction and characterization

DOC was extracted using solid-phase extraction (SPE) with PPL cartridges following established protocols (Dittmar et al., 2008; Lu et al., 2018; Lu and Liu, 2019a). Briefly, 50 mL of filtered water samples were first acidified with HCl to a pH of 2, and DOC was subsequently extracted using PPL cartridges (Agilent Bond Elut Priority Pollutant PPL cartridge, 500 mg). DOC extracts were eluted with four cartridge volumes of LC/MS grade methanol (ca. 10 mL), dried and re-constituted to a final volume of 1 mL with pure water and stored at 4 °C before further analysis. The recovery rates ranged from 30 to 90% depending on when the sample was collected.

The extracted DOC was analyzed using an Ion Mobility Quadrupole Time of Flight LC/MS (IM Q-TOF LC/MS, Agilent 6560) equipped with an orthogonal electrospray ionization (ESI) source, operating in both ESI+ and ESI− modes. Briefly, in ESI+ mode, the mobile phase consisted of water with 0.1% (*v*/v) formic acid as phase A, and acetonitrile as phase B. DOC samples (5–50 μL) were eluted through a StableBond C18 column (Poroshell 120 SB-C18; 2.7 μm, 2.1 × 100 mm; Agilent P/N 685775–902) at a flow rate of 0.5 mL/min. The gradient elution profile involved a gradual increase of mobile phase B from 3% to 90% over the first 15 min, followed by a constant hold at 90% from 15 to 20 min, and a return to 3% at 21 min. A post-run period of 4 min ensured column equilibration before the subsequent injection. For ESI− mode, the mobile phases included water with 10 mmol/L ammonium acetate as phase A, and acetonitrile as phase B. DOC solutions (5–50 μL) went through a HILIC column (2.7 μm, 15 cm × 4.6 mm SUPELCO) at a flow rate of 0.5 mL/min. The elution profile involved maintaining mobile phase B at 98% for the initial minute, followed by a decrease to 95% over the subsequent 9 min. A post-run period of 15 min was allocated for column equilibration before the next injection. Approximately 0.5–2 μg C of DOC samples were injected per analysis, and each sample was analyzed in duplicate to ensure reliability and reproducibility of results.

The mass spectrum data were collected using MassHunter LC/MS Data Acquisition software (Version B.07.00 and B.09.00) in both ESI− and ESI+ modes. Specific settings of the instrument can be found in the Supporting Information (SI).

Data analysis was performed using MassHunter Qualitative Analysis software (Version B.07.00, Service Pack 2) based on established methods (Lu et al., 2018, 2021, 2023; Lu and Liu, 2019a). The software's "Find by Molecular Feature" function facilitated the identification of potential compounds detected in the samples. To enhance accuracy, MS spectra were converted into centroid format, with noise thresholds set at 500 and 2000 for ESI+ and ESI− modes, respectively, while signal thresholds were set at 4000 and 9000 for ESI+ and ESI− modes, respectively. A blank subtraction was further performed by comparing the features found in experimental groups and blanks (including both experimental blanks and analytical blanks) prior to formula assignment. A mass inaccuracy tolerance of ≤1.5 ppm was applied for formula assignment. Given the absence of nitrogen and phosphorus in the experiment setups (including the artificial sea salt, pure water, and plastic formulations), compound formulas were exclusively analyzed based on carbon (C), hydrogen (H), and oxygen (O) composition. The software's "Generate Formulas" function was employed, considering exact mass and ^{13}C isotope abundance and spacing. Subsequently, the generated formulas underwent screening using custom R scripts, adhering to these fundamental criteria: (1) Double Bond Equivalent (DBE) = $1 + 1/2(2C - H) \geq 0$; (2) O:C ≤ 1; (3) $0.333 \leq H/C \leq 2.25$; and (4) isotopic spacing and abundance. Carbon-normalized DBE, or DBE/C, was calculated as:

$$DBE \Big/ C = \frac{1 + C - 0.5H}{C}$$

For each molecular formula, the aromaticity index (AI) was calculated using the equation:

$$AI = \frac{1 + C - 0.5O - 0.5H}{C - 0.5O}$$

with values falling between 0.5 and 0.67 designated as aromatic, and those exceeding 0.67 categorized as condensed aromatic structures (Koch and Dittmar, 2006). In addition, DOM molecules can be further assigned to different categories based with their different elemental stoichiometries (e.g., Kim et al., 2003; Lu et al., 2023; Lu and Liu, 2019b; Mangal et al., 2017, 2016; Ohno and Ohno, 2013): (I) lipid-like structures with elemental ratios of: $0.01 \leq O/C \leq 0.1$; $1.5 \leq H/C \leq 2.0$; (II) carbohydrate-like structures: $0.65 < O/C \leq 1.0$; $1.5 < H/C \leq 2.25$; and (III) carboxyl-rich alicyclic molecules (CRAM)-like compounds: ($0.30 \leq DBE/C \leq 0.68$; $0.2 \leq DBE/H \leq 0.95$; $0.77 \leq DBE/O \leq 1.75$).

All statistical analyses were performed using OriginPro 2025. Differences among groups were evaluated using one-way analysis of variance (ANOVA), followed by Tukey's post hoc test for multiple comparisons. A significant level of $p < 0.05$ was applied throughout.

3. Results

3.1. Photooxidation of nurdles

The weight of both PE and PC nurdles did not change significantly after the 8 weeks of incubation under either light or dark conditions ($p = 0.28$ for PE, $p = 0.32$ for PC, ANOVA). In addition, the appearance of PE nurdles remained largely unchanged after the sunlight exposure, whereas the PC nurdles became more yellowish with the light exposure time (Fig. S1). Consistently, previous studies have documented instances where plastic materials exhibited darkening or yellowing after exposure to sunlight/ultraviolet (UV) radiation (Jiang et al., 2021; Turner and

Holmes, 2011). This phenomenon is commonly attributed to photooxidation, whereby oxygen is integrated into the polymer backbone chain, resulting in the formation of chromophores and thus enhancing the polymer's coloration (Martí et al., 2020; Turner et al., 2020). In addition, photo-Fries rearrangement may have contributed to the coloration of PC (Collin et al., 2012; Factor and Chu, 1980).

FTIR spectra of nurdles at different exposure timepoints were obtained to monitor the extent of the photochemical reactions (Fig. S2). As expected, the spectra of nurdles incubated under dark remained largely unaltered (Fig. S2, B). In contrast, under light exposure, new peaks or functional groups were generated for both PE and PC nurdles, including hydroxyls (3300–3400 cm^{-1}), carbonyls (1690–1730 cm^{-1}), vinyl (alkenes, 1620–1650 cm^{-1}), and ethers (1100–1200 cm^{-1}).

Oxidation indices of nurdles were calculated based on the FTIR spectra (Fig. 1). Generally, the oxidation indices for both PE and PC nurdles increased steadily with exposure time, reaching maximum values at 6 and 8 weeks. The oxidation indices of PE nurdles increased from 0.02 ± 0.01 to 0.03 ± 0.01, 0.04 ± 0.03, 0.09 ± 0.03, 0.15 ± 0.05 ($p = 0.01$, *t*-test), and 0.21 ± 0.08 (p = 0.01, t-test), spanning from 1d to 1 week, 2 weeks, 4 weeks, 6 and 8 weeks of sunlight exposure, respectively. Similarly, the oxidation index of PC nurdles also increased from 1.58 ± 0.04 to 1.58 ± 0.03, 1.61 ± 0.05, 1.60 ± 0.06, 2.02 ± 0.12 ($p = 0.03$, t-test), and 2.11 ± 0.16 ($p = 0.02$, t-test), over the same exposure durations. The higher oxidation indices observed for PC nurdles primarily reflect their oxygen-containing polymer structure, which results in a higher baseline signal rather than enhanced photooxidation.

The individual indices of PE were dominated by the C═O bond throughout the exposure period, with a subsequent increase of the C—O bond after 4 weeks of exposure, indicating the presence of carbonyl and ether/ester groups, respectively. Conversely, for PC nurdles, the oxidation index was dominated by the C—O bond due to its inherent backbone structure, with a notable increase of C═O bond between 2 and 4 weeks. The oxidation indices for both PE and PC nurdles increased more greatly from 4 to 6 and 8 weeks, suggesting intensified oxidation reactions (Brandon et al., 2016), albeit with distinct oxidation degrees for PE and PC. Notably, the prevalence of the C═O bond in the oxidation index implied the predominance of Norrish-type reactions (Alimi et al., 2021), which might lead to the formation of carbonyl groups on the nurdle surface.

The DO concentration decreased over time in the light treatment but remained stable in the dark treatment (Fig. 2; note that this was a separate set of experiments from the nurdle photooxidation experiment in Figs. 1 & 3). The DO consumption in the dark treatment was minimal, with <1% depletion for both polymers over 2 weeks. However, under light exposure, oxygen concentrations for PE nurdles dropped from 143.14 μM at the start of the experiment to 22.83 ± 10.37 μM at week 1 and 2.30 ± 0.63 μM at week 2. Similarly, oxygen levels for PC nurdles decreased from 143.14 μM to 63.52 ± 3.74 μM at week 1 and 22.50 ± 6.19 μM at week 2. Over the 2-week period, 98% of the DO in the solution of PE nurdles and 84% in the solution of PC nurdles was consumed, indicating the heavy involvement of DO in photochemical reactions.

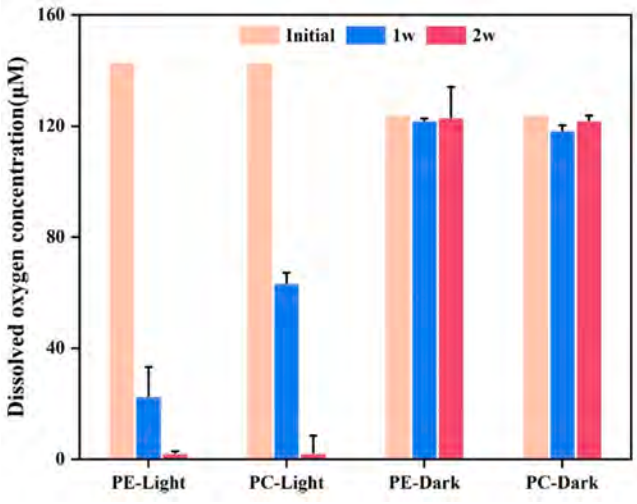

Fig. 2. Dissolved oxygen concentrations in artificial seawater during PE and PC nurdle incubation under light/dark treatment.

The amount of DO consumed is not directly comparable to the oxidation indices, DO consumption during photooxidation reflect multiple oxygen sinks, including incorporation into oxygen-containing functional groups on the plastic surface, incorporation into released DOC, and conversion to inorganic carbon. Without quantitative constraints on (i) the oxygen source (dissolved O_2 vs. water), (ii) the depth/extent of oxidation within the nurdle surface, and (iii) the oxygen content of the produced DOC, it is not feasible to construct a robust oxygen mass balance for the observed DO consumption.

3.2. Production of DOC

DOC was produced in both sunlight and dark incubations (Fig. 3, Tables 1 and 2). Under dark incubation, the concentrations of DOC

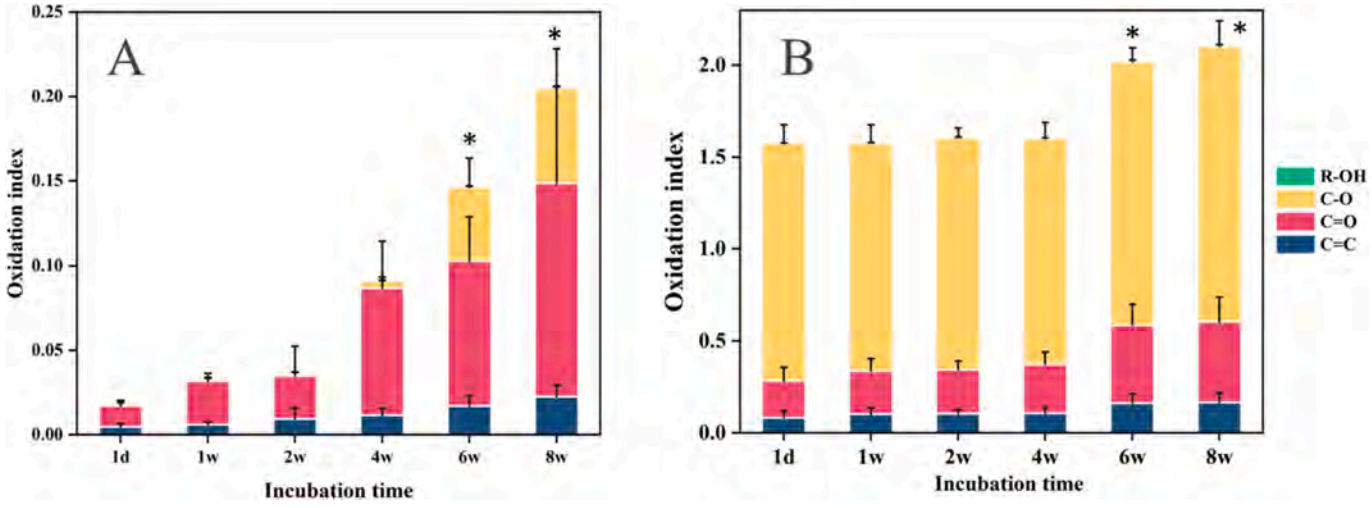

Fig. 1. Oxidation indices of PE (A) and PC (B) nurdles after simulated sunlight exposure, calculated by summing four individual bonds: R-OH (alcohol), C—O (ether), C═O (ketone), and C═C (vinyl).

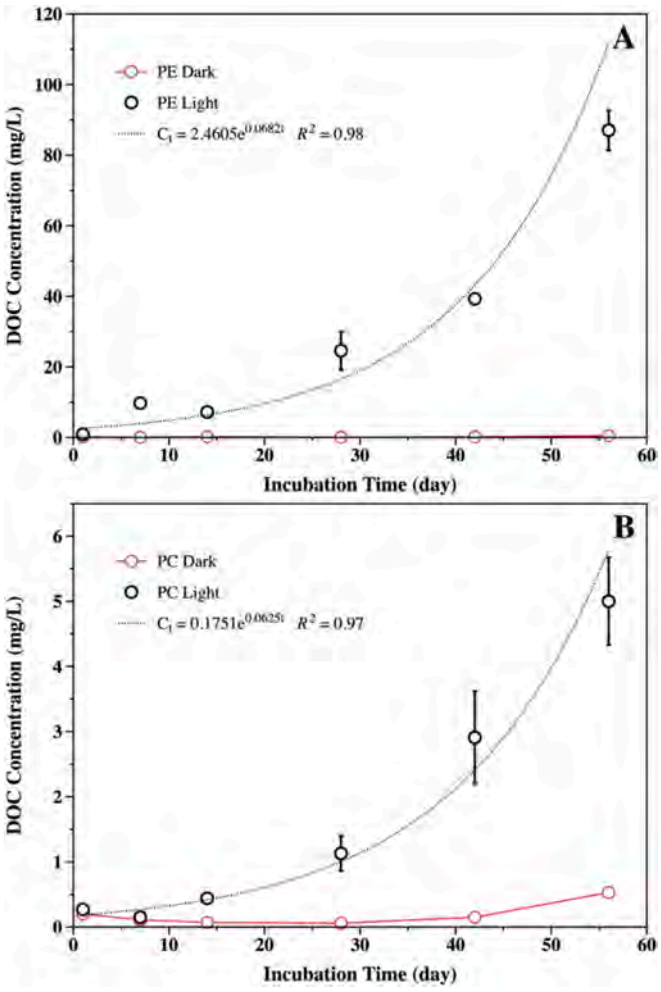

Fig. 3. Total dissolved organic carbon (TDOC) production from polyethylene (PE, A), and polycarbonate (PC, B) nurdles in artificial seawater in both light and the dark. Note that the y-axis scales differ between panels to accommodate the different concentration ranges between PE and PC.

remained low and relatively constant, with the highest concentration occurring at 8 weeks of incubation, but barely detectable after 1 day of incubation. The DOC concentrations of PE nurdles ranged from 0.17 ± 0.04 to 0.03 ± 0.02, 0.20 ± 0.06, 0.03 ± 0.00, 0.17 ± 0.09, and 0.48 ± 0.01 mg C/L from 1d to 1 week, 2 weeks, 4 weeks, 6 weeks, and 8 weeks of dark incubation, respectively. Similarly, the DOC concentrations of PC nurdles ranged from 0.20 ± 0.08 to 0.11 ± 0.01, 0.07 ± 0.01, 0.06 ± 0.03, 0.15 ± 0.02, and 0.53 ± 0.02 mg C/L over the same incubation duration.

In comparison to the dark controls, nurdles under sunlight exposure released much higher levels of DOC for both PE and PC nurdles over the same exposure period. The DOC concentrations of PE nurdles increased from 0.90 ± 0.02 to 9.73 ± 0.74, 7.21 ± 1.50, 24.59 ± 5.47, 39.27 ± 0.97, and 87.07 ± 5.67 mg C/L from 1d to 1 week, 2 weeks, 4 weeks, 6 weeks, and 8 weeks of sunlight exposure, respectively. Similarly, the DOC concentrations of PC nurdles increased from 0.27 ± 0.00 to 0.15 ± 0.05, 0.44 ± 0.05, 1.13 ± 0.27, 2.91 ± 0.71, and 5.00 ± 0.67 mg C/L over the same exposure duration. The DOC concentration curves for both PE and PC nurdles show an exponentially increasing pattern (Fig. 3), indicating accelerating production of DOC without reaching plateau within 8 weeks.

The photooxidation of PE nurdles not only consumed more DO but also produced more DOC than PC nurdles, reaching approximately 90 mg/L after 8 weeks of incubation — equivalent to 1% of the original PE nurdles by weight. In contrast, PC nurdles produced much less DOC, with only 5 mg/L after the 8 weeks. This disparity suggests the different environmental behaviors of PE and PC under sunlight exposure, likely due to their different chemical structures. The higher DO consumption and higher DOC release from PE nurdles indicate their more rapid photooxidation and thus the accelerated breakdown of the polymer chains.

Overall, sunlight exposure generated more DOC than dark incubation for both nurdles, consistent with studies showing that UV-induced plastic degradation increases DOC production by breaking polymer chains (Tian et al., 2019; Ward et al., 2019; Zhu et al., 2020b), highlighting the role of photochemical processes in accelerating plastic weathering and releasing plastic-derived compounds into marine environments.

3.3. Identification of possible nanoplastics

Across all samples, including the incubation solution of PE nurdles after 4, 6, and 8 weeks of sunlight exposure, and PC nurdles after 8 weeks of sunlight exposure, the DOC of the permeate, which passed through the ultrafiltration membrane (defined as ultrafiltered DOC), accounted for approximately 98.2–99.5% of the bulk (Table S1). This result showed that the leached compounds from PE and PC after sunlight exposure were truly dissolved (molecular weight < 3000 Da), or there was negligible production or < 0.2% of nanoplastics (> 3000 Da or > 1 nm).

Surface morphology analysis revealed no significant changes to the nurdles in the dark treatment (data not shown). However, roughness and small cracks were observed on the PE nurdles after 6 and 8 weeks of sunlight exposure, respectively (Fig. 4). Similarly, cracks were observed on PC nurdles after 8 weeks of sunlight exposure. These alterations confirm mechanical changes to the plastic surface following photooxidation. This observation aligns with the notable increase in oxidation indices observed at 6 and 8 weeks of sunlight exposure for both PE and PC nurdles (Fig. 1). However, there were no fragments observed within

Table 1
Element stoichiometry of CHO molecular formulas produced from PE during the photooxidation of nurdles in artificial seawater.

	Incubation time	1d	1w	2w	4w	6w	8w
	DOC-production (mg/L)	0.90 ± 0.02	9.73 ± 0.74	7.21 ± 1.50	24.59 ± 5.47	39.27 ± 0.97	87.07 ± 5.67
ESI+	Assigned formulas	93	328	335	372	77	97
	Average molecular mass	232.11 ± 65.86	306.61 ± 133.01	315.45 ± 127.07	232.99 ± 69.75	280.32 ± 134.53	266.43 ± 106.21
	Average H/C	1.59 ± 0.31	1.21 ± 0.41	1.08 ± 0.34	1.23 ± 0.42	1.23 ± 0.48	1.28 ± 0.50
	Average O/C	0.26 ± 0.15	0.19 ± 0.15	0.17 ± 0.11	0.27 ± 0.18	0.28 ± 0.32	0.47 ± 0.32
	Average AI	0.22 ± 0.17	0.39 ± 0.22	0.47 ± 0.19	0.39 ± 0.23	0.38 ± 0.29	0.30 ± 0.31
	Average DBE/C	0.30 ± 0.17	0.45 ± 0.20	0.51 ± 0.17	0.47 ± 0.21	0.45 ± 0.23	0.44 ± 0.23
ESI−	Assigned formulas	1	166	180	1596	2714	1863
	Average molecular mass	274.18	275.03 ± 149.14	291.52 ± 165.75	324.90 ± 146.88	342.00 ± 154.98	330.41 ± 156.21
	Average H/C	1.86	1.78 ± 0.18	1.67 ± 0.25	1.55 ± 0.32	1.46 ± 0.33	1.46 ± 0.41
	Average O/C	0.36	0.36 ± 0.12	0.40 ± 0.11	0.37 ± 0.13	0.41 ± 0.17	0.42 ± 0.18
	Average AI	0	0.04 ± 0.09	0.09 ± 0.14	0.15 ± 0.18	0.19 ± 0.19	0.20 ± 0.22
	Average DBE/C	0.14	0.20 ± 0.09	0.26 ± 0.14	0.30 ± 0.16	0.35 ± 0.16	0.36 ± 0.20

Table 2
Element stoichiometry of CHO molecular formulas produced from PC during the photooxidation of nurdles in artificial seawater.

	Incubation time	1d	1w	2w	4w	6w	8w
	DOC-production (mg/L)	0.27 ± 0.00	0.15 ± 0.05	0.44 ± 0.05	1.13 ± 0.27	2.91 ± 0.71	5.00 ± 0.67
ESI+	Assigned formulas	44	67	223	340	355	247
	Average molecular mass	265.39 ± 86.07	292.12 ± 97.37	289.96 ± 91.65	278.61 ± 96.20	274.31 ± 99.52	325.60 ± 121.02
	Average H/C	1.52 ± 0.38	1.48 ± 0.46	1.60 ± 0.40	1.51 ± 0.40	1.29 ± 0.38	1.23 ± 0.38
	Average O/C	0.31 ± 0.17	0.35 ± 0.16	0.34 ± 0.17	0.27 ± 0.14	0.22 ± 0.13	0.36 ± 0.32
	Average AI	0.24 ± 0.23	0.26 ± 0.24	0.19 ± 0.22	0.24 ± 0.23	0.36 ± 0.21	0.35 ± 0.23
	Average DBE/C	0.33 ± 0.21	0.34 ± 0.23	0.29 ± 0.21	0.32 ± 0.21	0.43 ± 0.19	0.45 ± 0.18
ESI−	Assigned formulas	nd	nd	nd	3	306	313
	Average molecular mass	nd	nd	nd	517.62 ± 267.97	256.23 ± 111.59	349.93 ± 209.81
	Average H/C	nd	nd	nd	1.96 ± 0.05	1.07 ± 0.27	0.99 ± 0.24
	Average O/C	nd	nd	nd	0.31 ± 0.03	0.46 ± 0.19	0.32 ± 0.13
	Average AI	nd	nd	nd	0	0.41 ± 0.21	0.51 ± 0.14
	Average DBE/C	nd	nd	nd	0.07 ± 0.03	0.56 ± 0.14	0.59 ± 0.12

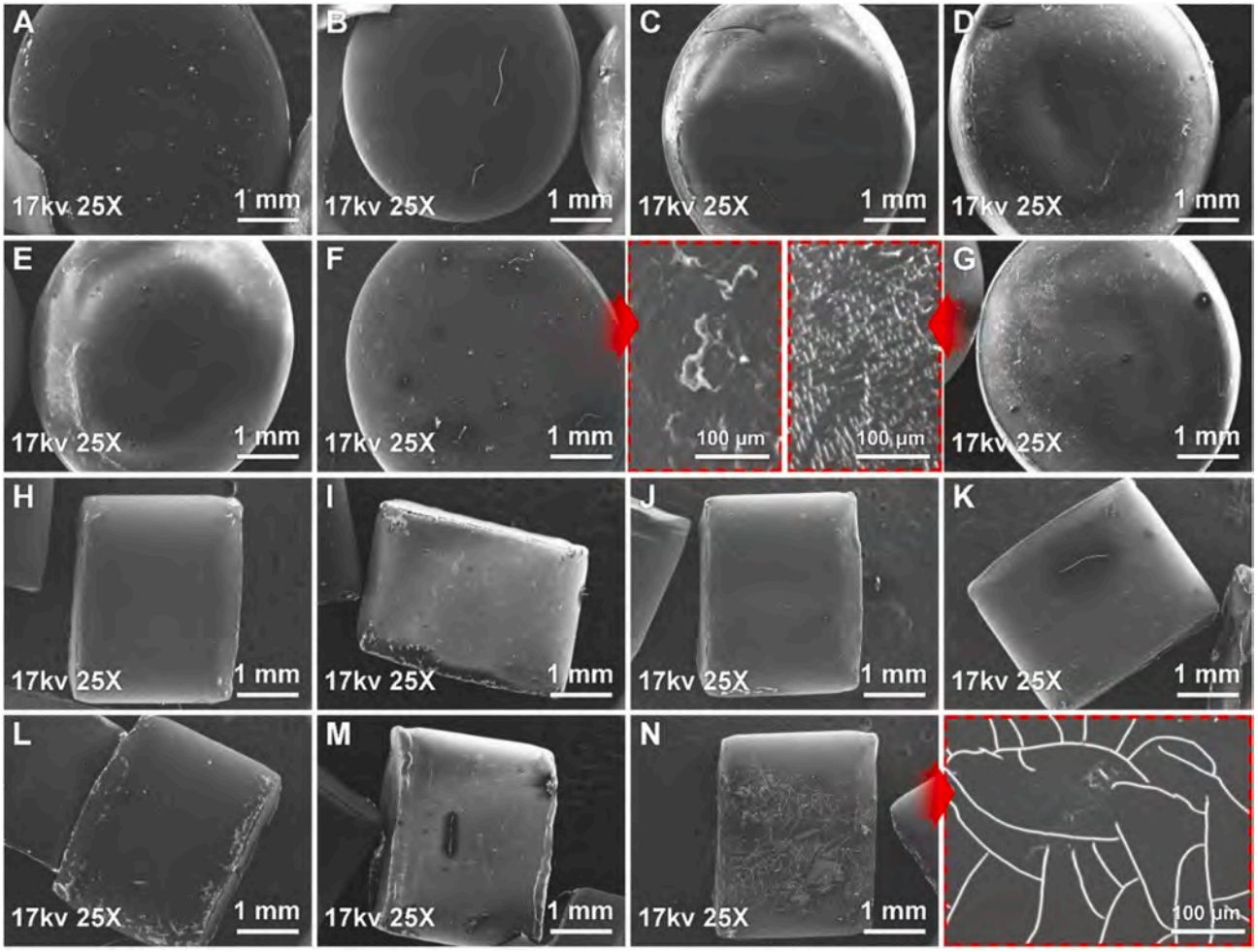

Fig. 4. SEM images of surface morphology with magnification of 25× by increasing sunlight exposure time for PE (A,B, C, D, E, F, G at 1d, 1w, 2w, 4w, 6w, 8w, respectively, with 300× magnification of 6w and 8w showing with red arrows) and PC (H, I, J, K, L, M, N at 1d, 1w, 2w, 4w, 6w, 8w, respectively, with 300× magnification of 8w showing with red arrow) nurdles. No fragments were observed within the resolution limits.

the cracks on PE or PC nurdles (Fig. 4), nor were detached particles in nanometer size range. This finding is consistent with the ultrafiltration results, where hardly any nanoplastics were detected in the leached DOC.

3.4. Extraction and molecular formulas of nurdle-derived DOC

The recovery rates of plastic-derived DOC through SPE varied greatly, ranging from 30% to 90%. Specifically, the recovery rates of PE-DOC after 2 weeks of incubation ranged from 30% to 40%, whereas after 4 weeks, they increased notably to between 70% and 90%. However, at 6 and 8 weeks of incubation, the recovery rates fluctuated between 50% and 70%. The recovery rate of DOC extraction is rather constant in natural waters, typically about 40–50%, depending on the water and specific laboratories (e.g., Dittmar et al., 2008). Since the exact same protocol was used for all the samples, the large variability observed is likely related to the compositional changes of plastic-derived DOC over time, with different compounds exhibiting varying affinities for the SPE

cartridges (PPL, Agilent). The PPL, made of a styrene-divinylbenzene polymer modified with a nonpolar surface, is designed to retain even the most polar classes of compounds, which may explain the higher recovery rates for the more polar DOC collected at the end of the incubation (details later).

Numerous formulas were assigned from the DOC of nurdles after incubation, from both dark and light treatments (Figs. S3, Tables 1, 2, and S2). In the dark treatment, due to low DOC concentrations, compounds were detected only at 1 day and 8 weeks of incubation. Most identified compounds from both PE and PC nurdles appeared in ESI+ mode, showing similar H/C and O/C ratios at both time points, suggesting gradual leaching of impurities or additives. However, some PE-derived compounds detected in ESI- mode after 8 weeks exhibited higher O/C ratios, indicating potential leaching of oxidized products, likely through radicals such as hydroxyls in natural waters (Zeng et al., 2023).

Under sunlight exposure, in total 9720 compounds were detected in the nurdle-derived DOC. More formulas were assigned in negative mode than in positive mode. The molecular masses of nurdle-derived DOC were small, ranging from 102 to 716 Da for negative mode and from 102 to 926 Da for positive mode. PE nurdles yielded more formulas than PC nurdles, consistent with the much higher levels of DOC production and thus more diverse DOC molecules (Fig. 5). From elemental stoichiometries, relatively low percentage of formulas (from all treatments) can be categorized into known biomolecules such as lipid- (2.1% under ESI+, 0.3% under ESI-) and carbohydrate-like compounds (3.3% under ESI+; 2.2% under ESI-), compared with CRAM-like compounds (11.6% under ESI+; 25.6% under ESI-), suggesting the leached out DOM was quite different from known biomolecules. Furthermore, while more compounds were detected in positive mode for both polymers at early exposure times (e.g., 1 day, 1 week, and 2 weeks of sunlight exposure, Tables 1 and 2), more compounds detected in negative mode occurred at 4 weeks, 6 weeks, and 8 weeks of sunlight exposure. A same trend was also observed for CRAM-like compounds, with the majority detected in the later stage of the incubations. This shift suggests that the property of nurdle-derived DOCs changed significantly in the middle of sunlight exposure period, likely a potential increase in acidic compounds such as those with carboxylic groups (details later), which are more readily ionized under negative ionization mode during the LC/MS analysis.

The composition and quantity of nurdle-derived DOCs differed greatly between PE and PC nurdles during the sunlight exposure, but the DOCs shared similar trends from their H/C and O/C ratios. For PE-derived DOCs, in positive mode, the average O/C ratio and DBE/C significantly increased at 6 and 8 weeks of exposure (from 0.22 at day 1 to 0.27 and 0.28 at 6 and 8 weeks, respectively, for O/C ratio, $p < 0.01$, ANOVA; from 0.3 to 0.45 and 0.44 for DBE/C, $p < 0.01$, ANOVA, respectively), accompanied by a decrease in the associated H/C ratios from 1.59 to 1.23 and 1.28 during the same period. In negative mode, this trend was more pronounced, with the average O/C ratio, AI, and DBE/C increasing over time (from 0.36 to 0.36, 0.40, 0.37, 0.41, and

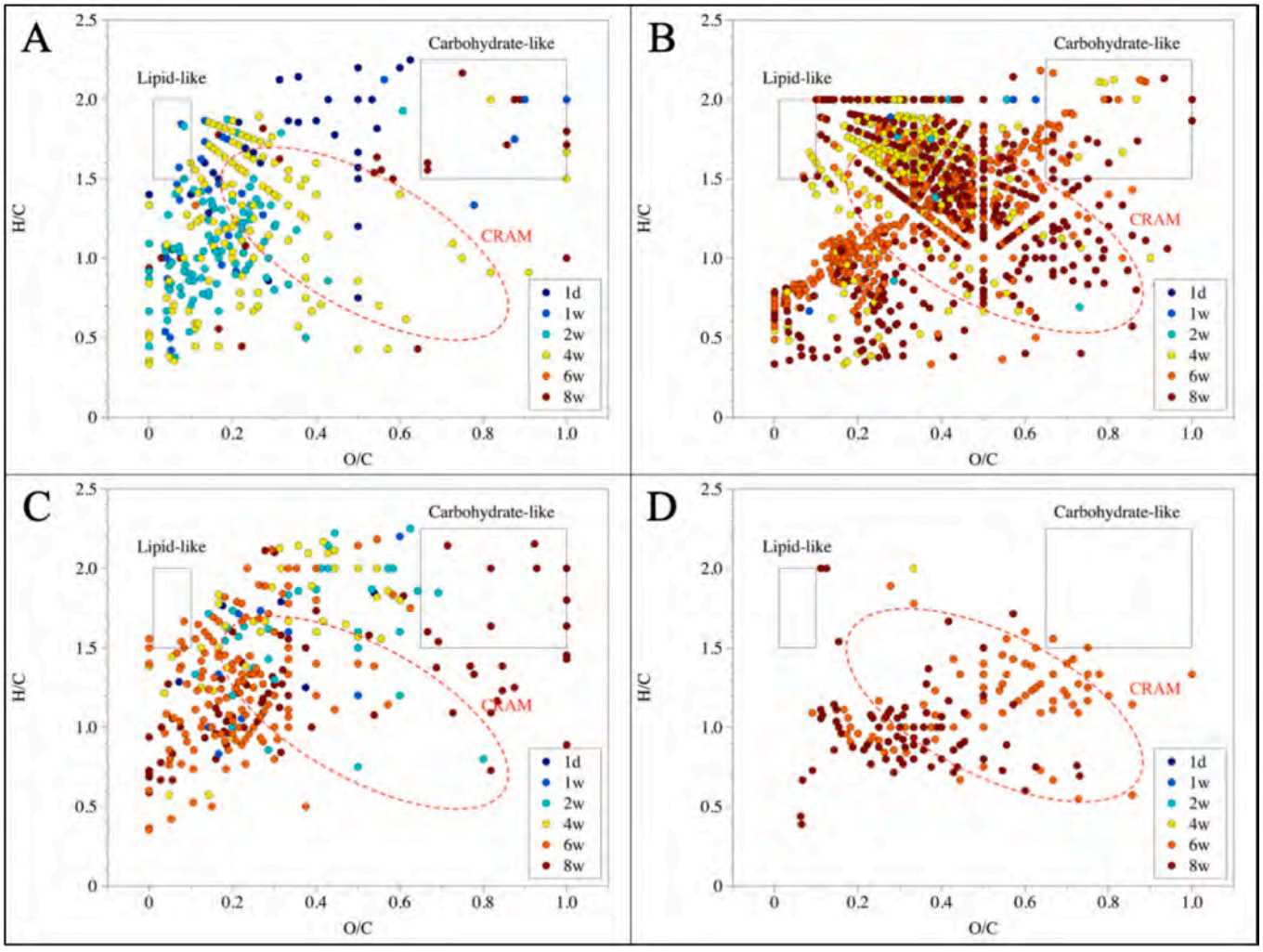

Fig. 5. van Krevelen diagrams for CHO molecular formulas produced during the photooxidation of nurdles in artificial seawater: (A) PE-derived DOCs under ESI+ mode; (B) PE-derived DOCs under ESI− mode; (C) PC-derived DOCs under ESI+ mode; (D) PC-derived DOCs under ESI− mode.

0.42 from 1d to 1w, 2w, 4w, 6w, and 8w of exposure for O/C ratio, $p < 0.01$, ANOVA; from 0 to 0.04, 0.09, 0.15, 0.19, and 0.20 for AI, $p < 0.01$, ANOVA; and from 0.14 to 0.20, 0.26, 0.30, 0.35, and 0.36 for DBE/C, $p < 0.01$, ANOVA, respectively), while the H/C ratio decreased (from 1.86 to 1.78, 1.67, 1.55, 1.46 and 1.46 from 1d to 1w, 2w, 4w, 6w, and 8w of exposure, $p < 0.01$, ANOVA, respectively). In contrast, for PC-derived DOCs, the high oxygen content in PC's backbone chain (various monomer formulas but all contain oxygen, e.g., $C_{14}H_{16}O_3$ and $C_{15}H_{16}O_2$) made it challenging to compare the O/C ratios. Nevertheless, in positive mode, the H/C ratio of PC-derived DOCs significantly decreased from 1.52 at day 1 to 1.29 and 1.23 at weeks 6 and 8 ($p < 0.01$, ANOVA), and consistently, the associated AI and DBE/C significantly increased during the same period (from 0.24 at 1 day to 0.36 and 0.35 at 6 and 8 weeks, respectively, for AI, $p < 0.01$, ANOVA; from 0.33 at 1 day to 0.43 and 0.45 at 6 and 8 weeks, respectively, for DBE/C, $p < 0.01$, ANOVA), indicating the increase of unsaturated bonds and aromatic-like structures in the plastic-derived DOCs as the light exposure proceeded.

4. Discussion

4.1. Photooxidation of PE and PC nurdles: The role of oxygen

Photooxidation of plastics typically initiates with the absorption of photons by the polymer, leading to the formation of free radicals (Ainali et al., 2021; Andrady, 2022; Kuzina and Mikhailov, 2001, 1998, 1993; Rånby, 1989). These radicals then engage in reactions with oxygen, triggering a cascade of oxidative chain reactions (Alimi et al., 2021). While different polymers share similar photooxidation principles, they may form radicals in distinct ways. For example, aromatic polymers such as PS and PC can directly absorb photons by their aromatic structures (Gewert et al., 2015). Conversely, aliphatic polyolefins like PP and PE lack functional moieties to absorb photons, thus impurities from the manufacturing process may serve as the source of the initial radicals for these types of polymers (Alimi et al., 2021).

Similar oxidative chain reactions have been observed in the photooxidation process of different polymers, resulting in the generation of same functional groups, such as carbonyl groups (Jiang et al., 2024). Consistently, our FTIR results showed the oxidation of both PE and PC nurdles after sunlight exposure (Fig. 1). The generation of C—O and C═O peaks are the typical reactive intermediates of Norrish-type reactions through the cleavage of carbon-carbon bonds upon exposure to light, leading to the incorporation of carbonyl groups into the polymer chains. However, PE nurdles were more oxidized than PC, evidenced by the increase in C—O moieties during later stages of exposure (e.g., 6 weeks and 8 weeks of sunlight exposure; Fig. 1). Moreover, the amounts of DOC production and DO consumption from these two polymers are consistent with the oxidation degree of the nurdle surface (Figs. 2&3). PE nurdles generated more DOCs than PC nurdles, by an 18-fold difference, and consumed more DO after the same duration of sunlight exposure. Note that the DO consumption experiment is an independent set of experiments from the DOC production ones, as the former was tightly sealed and without any headspace while the latter had extra DO input from the headspace and gentle shaking. Therefore, results from these two sets of experiments are not directly comparable quantitatively.

A slight increase in DOC at 8 weeks of incubation was observed under dark conditions (Fig. 3), which has been often attributed to the leaching of hydrophilic impurities and/or additives in the plastics (Romera-Castillo et al., 2018). Thus, the slight increase in DOC has been attributed to the release of low–molecular-weight species, residual processing compounds, and/or trace additives inherently present in polymer materials (Gewert, 2018; Guo et al., 2019), albeit at a much slower rate when without sunlight exposure. Biodegradation may have also contributed to this rise in DOC, considering that the dark incubation systems were not strictly sterile. However, thorough cleaning of nurdles and incubation glassware (combusted) as well as the use of artificial seawater (combusted sea salts) without inoculum minimizes the likelihood of significant microbial activity, if any.

It is often thought that aromatic plastics are more susceptible to photooxidation than pure aliphatic plastics, owing to their content of conjugated double bonds and aromatic rings (Gewert et al., 2015), facilitating the generation of reactive intermediates. However, our results did not support this assumption, as PE exhibited greater oxidation than PC. Given that both PE and PC nurdles were under identical light intensity and temperature, and that they were unaltered pre-products devoid of common additives, we propose that the difference in buoyancy between the two polymers may have played a key role. The density of PE is much lighter than PC as compared to water, and PE floated on water surface while PC sunk to the bottom of the water. This spatial separation may have influenced the oxygen accessibility, with PE nurdles at the air-water interface having greater access to atmospheric oxygen (i.e., O_2 in the head space) compared to PC nurdles at the bottom. This is consistent with our observation that 98% of the DO was consumed within 2 weeks for PE nurdles, compared to 84% for PC nurdles (Fig. 2). The DO might be depleted in our incubation system after 2 weeks. Despite briefly opening the lids each day to balance pressure, oxygen replenishment may have been insufficient for the submerged PC nurdles. In contrast, PE nurdles floating at the surface had more consistent access to oxygen from the headspace, promoting more extensive photooxidation. Additionally, the rate of photooxidation is affected by the oxygen concentration (Andrady, 2022), thus the buoyancy difference may have resulted in varying exposure to both UV radiation and dissolved oxygen, with PE nurdles receiving much higher doses of each. As a result, even though PC is an aromatic polymer, its photooxidation was less pronounced than that of aliphatic PE. Further experiment involved with floating PC (e.g., using a mesh to hold PC pellets near the water-air interface) is needed to verify this hypothesis. In addition, the coloration of PC may have also inhibited further photodegradation due to the shielding effect (Chen et al., 2023). Although PC is an aromatic polymer, commonly used in sunglasses and sunshade materials, its engineered structural property may have contributed to its lower photooxidation.

While aromatic polymers are generally considered more prone to photooxidation, much of the evidence for this viewpoint comes from studies on PS rather than other aromatic plastics like PC. PS microplastics are frequently reported to be highly susceptible to weathering and produce more leachates or DOC than polyolefins under similar conditions (Song et al., 2017, 2020; Ward et al., 2019; Zhu et al., 2020b). For example, Song et al. (2020, 2017) found that expanded PS (EPS) experienced fragmentation easily when exposed to sunlight, and Zhu et al. (2020a, 2020b) found that EPS produced more DOCs than PE and PP under same simulated sunlight exposure. However, EPS has a distinct structure compared to regular PS, containing air-filled bubbles that make it lightweight and more prone to fragmentation. In this study, we selected polymers with similar size, shape, and manufacturing processes to reduce potential structural differences and ensure more comparable results. Further investigations comparing expanded versus non-expanded polymers or examining degradation in air versus water environments will be crucial to better understanding the different photodegradation behaviors of aliphatic and aromatic plastics.

4.2. Little production of nanoplastics from the photooxidation of PE and PC

Sunlight exposure triggers oxidation reactions on plastics, potentially altering their mechanical integrity (Barnes et al., 2009; Menzel et al., 2022; Song et al., 2020). Previous studies have shown the production of nanoscale particles through fragmentation during the photodegradation of plastics such as PE, PP, and PS (Menzel et al., 2022; Song et al., 2020). Photooxidation leads to cross-linking and chain scission reactions on the plastic surface, gradually weakening and embrittling the material and potentially causing macro- and microfragmentation (Gewert et al., 2015; Karlsson et al., 2018). However,

after 8 weeks of accelerated sunlight exposure, we found that the predominant photooxidation products from PE and PC nurdles were truly dissolved compounds (< 3000 Da), with a negligible amount of nanoplastics (> 1 nm) present. This outcome may be attributed to several factors, such as the use of intact large nurdles, the absence of mechanical forces during the photooxidation process, as well as the relatively short incubation time in the solar simulator, as compared to natural conditions (e.g., Tang et al., 2022).

In related studies focusing on microplastic photodegradation, plastic materials were often trimmed or ground, potentially deteriorating their physical properties and favoring fragmentation (Menzel et al., 2022; Zhu et al., 2020a; Zhu et al., 2020b). Moreover, to mimic natural conditions, mechanical forces such as abrasion with sand or stirring with bars were frequently applied during light exposure (Song et al., 2020, 2017). In contrast, our study applied minimal agitation, i.e., gentle shaking by hands, and intact nurdles, which have larger dimensions (5 mm in diameter) compared to typical microplastics used in similar studies. In this study, the oxidation of nurdles may have increased the hydrophilicity of the surface based on the FTIR results, facilitating the dissolution of small, oxidized molecules into ambient solutions. However, this process relies solely on passive diffusion based on solubility, with small soluble compounds ending up in the solution. In contrast, nanoplastics, due to their larger size compared to the compounds, may have remained attached to the nurdles in the absence of necessary mechanical forces.

Limited fragmentation during photooxidation only process was also reported (Andrady, 2022; Tuttle et al., 2024), which is in line with our findings. For example, Svedin reported no fragmentation of low-density polyethylene (LDPE) and polypropylene (PP) under simulated sunlight exposure (Svedin, 2020). Similarly, Kalogerakis et al. (2017) found no fragmentation of PE and PP plastics after 6 months of natural solar weathering. Both experiments in these two studies were conducted without strong mechanical forces such as abrasions or continuous stirring. Consistently, our results show that without mechanical forces involved, there was essentially no nanoplastics produced from primary plastics under photooxidation. Further work applying different degrees of mechanical forces and on plastics on different weathering stages may be needed to gain a better understanding on how nanoplastics are formed in natural environments. It may also be important to explore how differences in natural sunlight exposure and accelerated irradiation affect mechanical degradation and nanoparticle formation under environmentally realistic conditions. Although only PE and PC were tested in this work, the results suggest that photooxidation alone does not necessarily lead to linear size transition from macro-, micro- to nanoplastics, rather from microplastics to truly dissolved organic matter in aquatic environments.

4.3. Molecular-level information of photooxidation products

HRMS analysis can elucidate the molecular information of plastic-derived DOCs, including their molecular weights and element compositions (Gewert et al., 2018; Stubbins et al., 2023; Walsh et al., 2021). The stoichiometry of DOCs differed between PE and PC nurdles, with PC-DOCs exhibiting higher oxygen content due to the presence of oxygen in PC chains. Over exposure time, the assigned formulas of DOCs from both nurdles showed an increase in O/C ratios but a decrease in H/C ratios, suggesting a progressive enrichment of oxygen in the DOC composition. This enrichment likely resulted from the incorporation of more oxygen into plastic chains, replacing hydrogen atoms through chain scission reactions induced by sunlight exposure (Jiang et al., 2024). Additional evidence, such as tandem MS data, can further elucidate the oxygen-containing functional groups. Consistently, the FTIR results revealed a gradual addition of oxygen to plastic chains with exposure time (Fig. 1). Furthermore, an increase in the number of formulas assigned in negative mode at later exposure stages indicated a rise in carboxylic acid products of nurdle-derived DOCs, contributing to the elevated oxygen content. Consistently, Gewert et al. (2018) identified chain scission products, primarily dicarboxylic acids, from plastic pellets following UV exposure. It has also been demonstrated that carboxylic and dicarboxylic acids are among the most prevalent and stable products of PE photodegradation, as their structures exhibit greater resilience to sunlight exposure compared to ketones, aldehydes, and alcohols (Fachrul et al., 2021), and certainly these products are more soluble as well.

The stoichiometry of nurdle-derived DOCs offers insight into their bioavailability. Some studies suggested that molecules with low hydrogen content, indicated by a low H/C ratio, are less readily available to microorganisms (Kim et al., 2006), with those possessing an H/C ratio $\leq$ 1.5 considered resistant to degradation (D'Andrilli et al., 2015). Therefore, the observed decrease in H/C ratio of nurdle-derived DOCs over the duration of sunlight exposure in both ESI modes may indicate an increase in their recalcitrance over time. Moreover, the concurrent increase of AI and DBE/C of the DOC formulas suggested the enrichment of CRAM-like compounds (Lu et al., 2021; Stubbins et al., 2023), which might affect the environmental behavior of nurdle-derived DOCs, including their residence time and bioavailability (Zhu et al., 2020b). Similar findings were reported by Stubbins et al. (2023), who identified CRAM-like formulas in PE, PP, and expanded polystyrene (EPS)-derived DOCs after sunlight exposure, highlighting their varying bioavailabilities for microbial degradation. The CRAM-like compounds are known to be refractory in aquatic environments (Hertkorn et al., 2006), suggesting that nurdle-derived DOCs may be less susceptible to biodegradation and more recalcitrant in nature. Further bioassay experiments are needed to evaluate the bioavailability of plastic-derived DOC.

4.4. Environmental implications

This study revealed the significant production of DOC from both PE and PC nurdles into the ambient water after sunlight exposure, with PE yielding 18 times more DOC than PC nurdles. Importantly, under the condition of minimal mechanical forces, the predominant form of nurdle-derived DOC from photooxidation was found to be truly dissolved compounds (< 1 nm), rather than plastic particles in nanometer scales. It should be noted that the measurement of nanoplastics (>1 nm) was based on DOC mass balance following ultrafiltration and carbon quantification, thus we cannot rule out the presence of polymeric particles below the detection threshold or those not retained effectively by ultrafiltration membranes. Molecular signatures of nurdle-derived DOCs were influenced by their polymer composition, yet displayed a shared trend characterized by an increase in CRAM-like and carboxylic acid structures with prolonged exposure time. This study also underscores the role of oxygen availability, influenced by plastic density, in shaping photodegradation pathways and highlights the efficacy of high-resolution mass spectrometry in analyzing plastic photodegradation products.

Even though the nurdles used in this work are environmentally relevant because of their widespread presence along the beaches worldwide, they contain little or no additives, different than most of the plastic debris in the environment which contain additives. Therefore, caution is needed when extrapolating the results to other types of plastic debris, although the fundamental processes should be generalizable. Also, artificial seawater was used in this work for a clean interpretation of the produced DOC from the nurdles. Natural seawater contains an appreciable amount of DOC, often in the levels of several to 10s of ppm in coastal waters, which would accelerate (with extra photosensitizer) or inhibit (shading or shielding) the photodegradation of nurdle-derived DOC. Nevertheless, the molecular characteristics of the plastics-derived DOC and their relationship with the type of polymer should remain robust.

Further research on photodegradation and environmental weathering products of plastics using raw plastic materials and complementary analytical approaches is needed for a comprehensive understanding

of the fate and impacts of plastic pollution in natural environments. Also needed is to evaluate bioavailability of plastic-derived DOC to microorganisms in marine environments.

CRediT authorship contribution statement

Xiangtao Jiang: Writing – original draft, Methodology, Investigation, Formal analysis, Data curation, Conceptualization. **Kaijun Lu:** Writing – review & editing, Methodology, Data curation. **Zhanfei Liu:** Writing – review & editing, Validation, Supervision, Resources, Project administration, Funding acquisition, Formal analysis, Conceptualization.

Declaration of competing interest

The authors declare no conflict of interest.

Acknowledgments

We thank Dr. Kenny Befus and Dr. Elizabeth Catlos for their help with the Low-Vacuum Scanning Electron Microscope. We thank Dr. Ryan Hladyniuk from the UTMSI Core Facility Lab for helping with LC/MS analysis. This work was supported by the Matagorda Bay Mitigation Trust (RFP# 2022-2023-1) and Texas Gulf Coast Research Center.

Appendix A. Supplementary data

Supplementary data to this article can be found online at https://doi.org/10.1016/j.marpolbul.2026.119505.

Data availability

The data in this study are available at: https://doi.org/10.6084/m9.figshare.31442230.

References

Acampora, H., Berrow, S., Newton, S., O'Connor, I., 2017. Presence of plastic litter in pellets from great cormorant (Phalacrocorax carbo) in Ireland. Mar. Pollut. Bull. 117, 512–514. https://doi.org/10.1016/j.marpolbul.2017.02.015.

Ainali, N.M., Bikiaris, D.N., Lambropoulou, D.A., 2021. Aging effects on low- and high-density polyethylene, polypropylene and polystyrene under UV irradiation: an insight into decomposition mechanism by Py-GC/MS for microplastic analysis. J. Anal. Appl. Pyrolysis, 105207. https://doi.org/10.1016/j.jaap.2021.105207.

Alimi, O.S., Claveau-Mallet, D., Kurusu, R.S., Lapointe, M., Bayen, S., Tufenkji, N., 2021. Weathering pathways and protocols for environmentally relevant microplastics and nanoplastics: what are we missing? J. Hazard. Mater., 126955 https://doi.org/10.1016/j.jhazmat.2021.126955.

Andrady, A.L., 2022. Weathering and fragmentation of plastic debris in the ocean environment. Mar. Pollut. Bull. 180, 113761. https://doi.org/10.1016/j.marpolbul.2022.113761.

Antunes, J.C., Frias, J.G.L., Micaelo, A.C., Sobral, P., 2013. Resin pellets from beaches of the Portuguese coast and adsorbed persistent organic pollutants. Estuar. Coast. Shelf Sci. 130, 62–69. https://doi.org/10.1016/j.ecss.2013.06.016.

Barnes, D.K.A., Galgani, F., Thompson, R.C., Barlaz, M., 2009. Accumulation and fragmentation of plastic debris in global environments. Philos. Trans. R. Soc. B 364, 1985–1998. https://doi.org/10.1098/rstb.2008.0205.

Biber, N.F.A., Foggo, A., Thompson, R.C., 2019. Characterising the deterioration of different plastics in air and seawater. Mar. Pollut. Bull. 141, 595–602. https://doi.org/10.1016/j.marpolbul.2019.02.068.

Brandon, J., Goldstein, M., Ohman, M.D., 2016. Long-term aging and degradation of microplastic particles: comparing in situ oceanic and experimental weathering patterns. Mar. Pollut. Bull. 110, 299–308. https://doi.org/10.1016/j.marpolbul.2016.06.048.

Carpenter, E.J., Smith, K.L., 1972. Plastics on the Sargasso Sea surface. Science 175, 1240–1241.

Chen, Q., Allgeier, A., Yin, D., Hollert, H., 2019. Leaching of endocrine disrupting chemicals from marine microplastics and mesoplastics under common life stress conditions. Environ. Int. 130, 104938. https://doi.org/10.1016/j.envint.2019.104938.

Chen, Z., Sarakha, M., Christmann, J., 2023. Consequences of sequential photooxidation of polycarbonate: relating microscopic modifications to the change of oxygen permeability. J. Appl. Polym. Sci. 140, e54397. https://doi.org/10.1002/app.54397.

Clukey, K.E., Lepczyk, C.A., Balazs, G.H., Work, T.M., Lynch, J.M., 2017. Investigation of plastic debris ingestion by four species of sea turtles collected as bycatch in pelagic Pacific longline fisheries. Mar. Pollut. Bull. https://doi.org/10.1016/j.marpolbul.2017.04.064.

Collin, S., Bussière, P.-O., Thérias, S., Lambert, J.-M., Perdereau, J., Gardette, J.-L., 2012. Physicochemical and mechanical impacts of photo-ageing on bisphenol a polycarbonate. Polym. Degrad. Stab. 97, 2284–2293. https://doi.org/10.1016/j.polymdegradstab. 2012.07.036.

D'Andrilli, J., Cooper, W.T., Foreman, C.M., Marshall, A.G., 2015. An ultrahigh-resolution mass spectrometry index to estimate natural organic matter lability. Rapid Commun. Mass Spectrom. 29, 2385–2401. https://doi.org/10.1002/rcm.7400.

de Vos, A., Aluwihare, L., Youngs, S., DiBenedetto, M.H., Ward, C.P., Michel, A.P.M., Colson, B.C., Mazzotta, M.G., Walsh, A.N., Nelson, R.K., Reddy, C.M., James, B.D., 2021. The M/V X-Press Pearl Nurdle Spill: contamination of Burnt Plastic and Unburnt Nurdles along Sri Lanka's beaches. ACS Environ. Au. https://doi.org/10.1021/acsenvironau.1c00031.

Dittmar, T., Koch, B., Hertkorn, N., Kattner, G., 2008. A simple and efficient method for the solid-phase extraction of dissolved organic matter (SPE-DOM) from seawater. Limnol. Oceanogr. Methods 6, 230–235.

Egea, L.G., Brun, F.G., Jiménez-Ramos, R., 2024. Dissolved organic carbon leaching from microplastics and bioavailability in coastal ecosystems. Sci. Total Environ. 909, 168673. https://doi.org/10.1016/j.scitotenv.2023.168673.

Endo, S., Takizawa, R., Okuda, K., Takada, H., Chiba, K., Kanehiro, H., Ogi, H., Yamashita, R., Date, T., 2005. Concentration of polychlorinated biphenyls (PCBs) in beached resin pellets: variability among individual particles and regional differences. Mar. Pollut. Bull. 50, 1103–1114. https://doi.org/10.1016/j.marpolbul.2005.04.030.

Fachrul, M.F., Rinanti, A., Salmiati, S., Sunaryo, T., 2021. Degradation of polyethylene plastic waste by indigenous microbial consortium and Fungi. Indonesian Journal of Urban and Environmental Technology 5, 86–103. https://doi.org/10.25105/urbanenvirotech.v5i1.10749.

Factor, A., Chu, M.L., 1980. The role of oxygen in the photo-ageing of bisphenol-a polycarbonate. Polym. Degrad. Stab. 2, 203–223. https://doi.org/10.1016/0141-3910(80)90029-4.

Fotopoulou, K.N., Karapanagioti, H.K., 2012. Surface properties of beached plastic pellets. Mar. Environ. Res. 81, 70–77. https://doi.org/10.1016/j.marenvres.2012.08.010.

Gewert, B., 2018. Chemical Pollutants Released to the Marine Environment by Degradation of Plastic Debris.

Gewert, B., Plassmann, M.M., MacLeod, M., 2015. Pathways for degradation of plastic polymers floating in the marine environment. Environ Sci Process Impacts 17, 1513–1521. https://doi.org/10.1039/C5EM00207A.

Gewert, B., Plassmann, M., Sandblom, O., MacLeod, M., 2018. Identification of chain scission products released to water by plastic exposed to ultraviolet light. Environ. Sci. Technol. Lett. https://doi.org/10.1021/acs.estlett.8b00119.

Gregory, M.R., 2009. Environmental implications of plastic debris in marine settings—entanglement, ingestion, smothering, hangers-on, hitch-hiking and alien invasions. Philosophical Transactions of the Royal Society B: Biological Sciences 364, 2013–2025. https://doi.org/10.1098/rstb.2008.0265.

Guo, H., Zheng, X., Ru, S., Luo, X., Mai, B., 2019. The leaching of additive-derived flame retardants (FRs) from plastics in avian digestive fluids: the significant risk of highly lipophilic FRs. J. Environ. Sci. 85, 200–207. https://doi.org/10.1016/j.jes.2019.06.013. SI: Recent advances in Environmental Sciences.

Hammer, J., Kraak, M.H.S., Parsons, J.R., 2012. Plastics in the marine environment: the dark side of a modern gift. Rev. Environ. Contam. Toxicol. 220, 1–44. https://doi.org/10.1007/978-1-4614-3414-6_1.

Hansell, D.A., Carlson, C.A., 2014. Biogeochemistry of Marine Dissolved Organic Matter. Academic press.

Hertkorn, N., Benner, R., Frommberger, M., Schmitt-Kopplin, P., Witt, M., Kaiser, K., Kettrup, A., Hedges, J.I., 2006. Characterization of a major refractory component of marine dissolved organic matter. Geochim. Cosmochim. Acta 70, 2990–3010. https://doi.org/10.1016/j.gca.2006.03.021.

Jiang, X., Lu, K., Tunnell, J.W., Liu, Z., 2021. The impacts of weathering on concentration and bioaccessibility of organic pollutants associated with plastic pellets (nurdles) in coastal environments. Mar. Pollut. Bull. 170, 112592. https://doi.org/10.1016/j.marpolbul.2021.112592.

Jiang, X., Conner, N., Lu, K., Tunnell, J.W., Liu, Z., 2022. Occurrence, distribution, and associated pollutants of plastic pellets (nurdles) in coastal areas of South Texas. Sci. Total Environ. 842, 156826. https://doi.org/10.1016/j.scitotenv.2022.156826.

Jiang, X., Gallager, S., Pàmies, R.P., Ruff, S.E., Liu, Z., 2024. Laboratory-simulated Photoirradiation reveals strong resistance of primary macroplastics to weathering. Environ. Sci. Technol. 58, 14775–14785. https://doi.org/10.1021/acs.est.3c09891.

Kalogerakis, N., Karkanorachaki, K., Kalogerakis, G.C., Triantafyllidi, E.I., Gotsis, A.D., Partsinevelos, P., Fava, F., 2017. Microplastics generation: onset of fragmentation of polyethylene films in marine environment Mesocosms. Front. Mar. Sci. 4. https://doi.org/10.3389/fmars.2017.00084.

Karlsson, T.M., Hassellöv, M., Jakubowicz, I., 2018. Influence of thermooxidative degradation on the in situ fate of polyethylene in temperate coastal waters. Mar. Pollut. Bull. 135, 187–194. https://doi.org/10.1016/j.marpolbul.2018.07.015.

Kim, S., Kramer, R.W., Hatcher, P.G., 2003. Graphical method for analysis of ultrahigh-resolution broadband mass spectra of natural organic matter, the Van Krevelen diagram. Anal. Chem. 75, 5336–5344. https://doi.org/10.1021/ac034415p.

Kim, S., Kaplan, L.A., Hatcher, P.G., 2006. Biodegradable dissolved organic matter in a temperate and a tropical stream determined from ultra-high resolution mass spectrometry. Limnol. Oceanogr. 51, 1054–1063. https://doi.org/10.4319/lo.2006.51.2.1054.

Koch, B.P., Dittmar, T., 2006. From mass to structure: an aromaticity index for high-resolution mass data of natural organic matter. Rapid Commun. Mass Spectrom. 20, 926–932. https://doi.org/10.1002/rcm.2386.
Kuman, B.S.K., Chari, N.V.H.K., Reddy, K.K., Cheriyan, E., Sherin, C.K., Rao, D.B., Elangovan, S.S., Reddy, B.B., Gupta, G.V.M., 2024. Natural light driven plastic leaching effects on carbon chemistry in the tropical coastal waters of eastern Arabian Sea: an experimental study. Environ. Pollut. 362, 124948. https://doi.org/10.1016/j.envpol.2024.124948.
Kuzina, S.I., Mikhailov, A.I., 1993. The photo-oxidation of polymers—1. Initiation of polystyrene photo-oxidation. Eur. Polym. J. 29, 1589–1594. https://doi.org/10.1016/0014-3057(93)90250-J.
Kuzina, S.I., Mikhailov, A.I., 1998. Photo-oxidation of polymers—2. Photo-chain reaction of peroxide radicals in polystyrene. Eur. Polym. J. 34, 291–299. https://doi.org/10.1016/S0014-3057(97)00169-9.
Kuzina, S.I., Mikhailov, A.I., 2001. Photo-oxidation of polymers 4. The dual mechanism of polystyrene photo-oxidation: a hydroperoxide and a photochain one. Eur. Polym. J. 37, 2319–2325. https://doi.org/10.1016/S0014-3057(01)00028-3.
Lambert, S., Wagner, M., 2016. Formation of microscopic particles during the degradation of different polymers. Chemosphere 161, 510–517. https://doi.org/10.1016/j.chemosphere.2016.07.042.
Lee, Y.K., Murphy, K.R., Hur, J., 2020. Fluorescence signatures of dissolved organic matter leached from microplastics: polymers and additives. Environ. Sci. Technol. 54, 11905–11914. https://pubs.acs.org/doi/10.1021/acs.est.0c00942.
Li, Y., Lu, Z., Abrahamsson, D.P., Song, W., Yang, C., Huang, Q., Wang, J., 2022. Non-targeted analysis for organic components of microplastic leachates. Sci. Total Environ. 816, 151598. https://doi.org/10.1016/j.scitotenv.2021.151598.
Lu, K., Liu, Z., 2019a. Molecular level analysis reveals changes in chemical composition of dissolved organic matter from South Texas Rivers after high flow events. Front. Mar. Sci. 6. https://doi.org/10.3389/fmars.2019.00673.
Lu, K., Liu, Z., 2019b. Molecular level analysis reveals changes in chemical composition of dissolved organic matter from South Texas rivers after high flow events. Front. Mar. Sci. 6. https://doi.org/10.3389/fmars.2019.00673.
Lu, K., Gardner, W.S., Liu, Z., 2018. Molecular structure characterization of riverine and coastal dissolved organic matter with ion mobility quadrupole time-of-flight LCMS (IM Q-TOF LCMS). Environ. Sci. Technol. 52, 7182–7191. https://doi.org/10.1021/acs.est.8b00999.
Lu, K., Li, X., Chen, H., Liu, Z., 2021. Constraints on isomers of dissolved organic matter in aquatic environments: insights from ion mobility mass spectrometry. Geochim. Cosmochim. Acta 308, 353–372. https://doi.org/10.1016/j.gca.2021.05.007.
Lu, K., Xue, J., Guo, L., Liu, Z., 2023. The bio- and thermal lability of dissolved organic matter as revealed by high-resolution mass spectrometry and thermal chemical analyses. Mar. Chem. 250, 104184. https://doi.org/10.1016/j.marchem.2022.104184.
Mangal, V., Stock, N.L., Guéguen, C., 2016. Molecular characterization of phytoplankton dissolved organic matter (DOM) and sulfur components using high resolution Orbitrap mass spectrometry. Anal. Bioanal. Chem. 408, 1891–1900. https://doi.org/10.1007/s00216-015-9295-9.
Mangal, V., Shi, Y.X., Guéguen, C., 2017. Compositional changes and molecular transformations of dissolved organic matter during the arctic spring floods in the lower Churchill watershed (northern Manitoba, Canada). Biogeochemistry 136, 151–165. https://doi.org/10.1007/s10533-017-0388-8.
Martí, E., Martin, C., Galli, M., Echevarría, F., Duarte, C.M., Cózar, A., 2020. The colors of the ocean plastics. Environ. Sci. Technol. https://doi.org/10.1021/acs.est.9b06400 acs.est.9b06400.
Menzel, T., Meides, N., Mauel, A., Mansfeld, U., Kretschmer, W., Kuhn, M., Herzig, E.M., Altstädt, V., Strohriegl, P., Senker, J., Ruckdäschel, H., 2022. Degradation of low-density polyethylene to nanoplastic particles by accelerated weathering. Sci. Total Environ. 826, 154035. https://doi.org/10.1016/j.scitotenv.2022.154035.
Ohno, T., Ohno, P.E., 2013. Influence of heteroatom pre-selection on the molecular formula assignment of soil organic matter components determined by ultrahigh resolution mass spectrometry. Anal. Bioanal. Chem. 405, 3299–3306. https://doi.org/10.1007/s00216-013-6734-3.
Rånby, B., 1989. Photodegradation and photo-oxidation of synthetic polymers. J. Anal. Appl. Pyrolysis 15, 237–247. https://doi.org/10.1016/0165-2370(89)85037-5.
Romera-Castillo, C., Birnstiel, S., Álvarez-Salgado, X.A., Sebastián, M., 2022. Aged plastic leaching of dissolved organic matter is two orders of magnitude higher than virgin plastic leading to a strong uplift in marine microbial activity. Front. Mar. Sci. 9. https://doi.org/10.3389/fmars.2022.861557.
Romera-Castillo, C., Pinto, M., Langer, T.M., Álvarez-Salgado, X.A., Herndl, G.J., 2018. Dissolved organic carbon leaching from plastics stimulates microbial activity in the ocean. Nat. Commun. 9, 1430. https://doi.org/10.1038/s41467-018-03798-5.
Ryan, P.G., 1988. Effects of ingested plastic on seabird feeding: evidence from chickens. Mar. Pollut. Bull. 19, 125–128. https://doi.org/10.1016/0025-326X(88)90708-4.
Sewwandi, M., Keerthanan, S., Perera, K.I., Vithanage, M., 2023. Plastic Nurdles in marine environments due to accidental spillage. In: Microplastics in the Ecosphere. John Wiley & Sons, Ltd, pp. 415–432. https://doi.org/10.1002/9781119879534.ch26.
Song, Y.K., Hong, S.H., Jang, M., Han, G.M., Jung, S.W., Shim, W.J., 2017. Combined effects of UV exposure duration and mechanical abrasion on microplastic fragmentation by polymer type. Environ. Sci. Technol. 51, 4368–4376. https://doi.org/10.1021/acs.est.6b06155.
Song, Y.K., Hong, S.H., Eo, S., Han, G.M., Shim, W.J., 2020. Rapid production of micro- and nanoplastics by fragmentation of expanded polystyrene exposed to sunlight. Environ. Sci. Technol. https://doi.org/10.1021/acs.est.0c02288.
Stolpe, B., Guo, L., Shiller, A.M., Hassellöv, M., 2010. Size and composition of colloidal organic matter and trace elements in the Mississippi River, Pearl River and the northern Gulf of Mexico, as characterized by flow field-flow fractionation. Mar. Chem. 118, 119–128. https://doi.org/10.1016/j.marchem.2009.11.007.
Stubbins, A., Zhu, L., Zhao, S., Spencer, R.G.M., Podgorski, D.C., 2023. Molecular signatures of dissolved organic matter generated from the Photodissolution of microplastics in sunlit seawater. Environ. Sci. Technol. 57, 20097–20106. https://doi.org/10.1021/acs.est.1c03592.
Svedin, J., 2020. Photodegradation of Macroplastics to Microplastics : A Laboratory Study on Common Litter Found in Urban Areas.
Tang, C.-C., Chen, Y.-T., Zhang, Y.-M., Chen, H.-I., Brimblecombe, P., Lee, C.-L., 2022. Cracking and photo-oxidation of Polyoxymethylene degraded in terrestrial and simulated marine environments. Front. Mar. Sci. 9. https://doi.org/10.3389/fmars.2022.843295.
Tian, L., Chen, Q., Jiang, W., Wang, L., Xie, H., Kalogerakis, N., Ma, Y., Ji, R., 2019. A carbon-14 radiotracer-based study on the phototransformation of polystyrene nanoplastics in water versus in air. Environ. Sci. Nano 6, 2907–2917. https://doi.org/10.1039/C9EN00662A.
Tunnell, J.W., Dunning, K.H., Scheef, L.P., Swanson, K.M., 2020. Measuring plastic pellet (nurdle) abundance on shorelines throughout the Gulf of Mexico using citizen scientists: establishing a platform for policy-relevant research. Mar. Pollut. Bull. 151, 110794. https://doi.org/10.1016/j.marpolbul.2019.110794.
Turner, A., Holmes, L., 2011. Occurrence, distribution and characteristics of beached plastic production pellets on the island of Malta (Central Mediterranean). Mar. Pollut. Bull. 62, 377–381. https://doi.org/10.1016/j.marpolbul.2010.09.027.
Turner, A., Arnold, R., Williams, T., 2020. Weathering and persistence of plastic in the marine environment: lessons from LEGO. Environ. Pollut. 262, 114299. https://doi.org/10.1016/j.envpol.2020.114299.
Tuttle, E., Wiman, C., Muñoz, S., Law, K.L., Stubbins, A., 2024. Sunlight-driven photochemical removal of polypropylene microplastics from surface waters follows linear kinetics and does not result in fragmentation. Environ. Sci. Technol. 58, 5461–5471. https://doi.org/10.1021/acs.est.3c07161.
Walsh, A.N., Reddy, C.M., Niles, S.F., McKenna, A.M., Hansel, C.M., Ward, C.P., 2021. Plastic formulation is an emerging control of its photochemical fate in the ocean. Environ. Sci. Technol. 55, 12383–12392. https://doi.org/10.1021/acs.est.1c02272.
Wang, Q., Leonce, B., Seeley, M.E., Adegboyega, N.F., Lu, K., Hockaday, W.C., Liu, Z., 2020. Elucidating the formation pathway of photo-generated asphaltenes from light Louisiana sweet crude oil after exposure to natural sunlight in the Gulf of Mexico. Org. Geochem. 150, 104126. https://doi.org/10.1016/j.orggeochem.2020.104126.
Ward, C.P., Armstrong, C.J., Walsh, A.N., Jackson, J.H., Reddy, C.M., 2019. Sunlight converts polystyrene to carbon dioxide and dissolved organic carbon. Environ. Sci. Technol. Lett. https://doi.org/10.1021/acs.estlett.9b00532.
Zeng, G., Shi, M., Dai, M., Zhou, Q., Luo, H., Lin, L., Zang, K., Meng, Z., Pan, X., 2023. Hydroxyl radicals in natural waters: light/dark mechanisms, changes and scavenging effects. Sci. Total Environ. 868, 161533. https://doi.org/10.1016/j.scitotenv.2023.161533.
Zhang, W., Ma, X., Zhang, Z., Wang, Y., Wang, J., Wang, J., Ma, D., 2015. Persistent organic pollutants carried on plastic resin pellets from two beaches in China. Mar. Pollut. Bull. 99, 28–34. https://doi.org/10.1016/j.marpolbul.2015.08.002.
Zhu, K., Jia, H., Sun, Y., Dai, Y., Zhang, C., Guo, X., Wang, T., Zhu, L., 2020a. Long-term phototransformation of microplastics under simulated sunlight irradiation in aquatic environments: roles of reactive oxygen species. Water Res. 173, 115564. https://doi.org/10.1016/j.watres.2020.115564.
Zhu, L., Zhao, S., Bittar, T.B., Stubbins, A., Li, D., 2020b. Photochemical dissolution of buoyant microplastics to dissolved organic carbon: rates and microbial impacts. J. Hazard. Mater. 383, 121065. https://doi.org/10.1016/j.jhazmat.2019.121065.